

Laboratory experiment on rip current circulations over a moveable bed: Drifter measurements

B. Castelle,¹ H. Michallet,² V. Marieu,¹ F. Leckler,¹ B. Dubardier,¹ A. Lambert,^{2,3} C. Berni,² P. Bonneton,¹ E. Barthélemy,² and F. Bouchette³

Received 15 April 2010; revised 10 August 2010; accepted 15 September 2010; published 2 December 2010.

[1] This study describes a laboratory experiment on rip current circulations over a moveable bed. Rip current characteristics over eight contrasting nature-like beach morphologies are investigated. The seabed varied from reasonably alongshore uniform to strongly alongshore nonuniform with crescentic patterns and bar-rip morphologies, representative of a full morphological down-state sequence. The same offshore shore-normal waves were generated by the wavemaker for the eight situations with the same mean water level to study the sensitivity of rip current characteristics as a function of the beach morphology only. In each case, a 30 to 60 min video run was used to track a large number of drifters released within the surf zone. Results show the presence of classic rip current patterns with counterrotating cells and a relatively narrow offshore-directed jet varying from shore-normal to strongly skewed. Wave-driven circulations were strongly unstable. Computed standard deviations of flow intensity and direction provide high-resolution information on the spatial variability of rip current instabilities. Highly pulsating and weakly directionally variable offshore-directed flow is observed in the rip neck for well-developed bar-rip morphologies that turns into a weakly pulsating and highly directional variable rip current flow with decreasing beach alongshore nonuniformity. Proposing a definition of rip current intensity based on the rip current circulation geometry, rip current intensity was found to linearly increase with increasing measure of beach alongshore nonuniformity within both the low-energy and moderate-energy rip current regimes. To date, our laboratory experiment provides the first extensive quantitative rip current information during a full down-state sequence for a given wave condition.

Citation: Castelle, B., H. Michallet, V. Marieu, F. Leckler, B. Dubardier, A. Lambert, C. Berni, P. Bonneton, E. Barthélemy, and F. Bouchette (2010), Laboratory experiment on rip current circulations over a moveable bed: Drifter measurements, *J. Geophys. Res.*, 115, C12008, doi:10.1029/2010JC006343.

1. Introduction

[2] Rip currents are narrow, intense seaward flowing jets that originate within the surf zone and broaden outside the breaking zone. These ubiquitous flow patterns along wave-dominated beaches have been observed by coastal scientists for many years [Shepard *et al.*, 1941; McKenzie, 1958; Sonu, 1972]. In recent years, rip currents have received increasing interest [MacMahan *et al.*, 2008; Reniers *et al.*, 2009; Scott *et al.*, 2009; Bruneau *et al.*, 2009b; MacMahan *et al.*, 2010; Austin *et al.*, 2010; Reniers *et al.*, 2010]. They are associated with cell circulations, also known as rip current circulations. These nearshore circulations are thought to produce a continuous interchange between the waters of the surf

zone and the shelf, acting as both a distributing mechanism for nutrients and a dispersing mechanism for land runoff.

[3] Rip current circulations permanently interact with the surf zone sandbars and shoreline rhythms. The positive feedback between these wave-driven circulations, sediment processes and the evolving morphology leads to the development of striking nearshore patterns [Falqués *et al.*, 2000] that are the so-called crescentic sandbars [Van Enckevort *et al.*, 2004; Castelle *et al.*, 2007] and bar-rip morphologies [Holman *et al.*, 2006]. These three-dimensional (3-D) morphological rhythmic or quasi-rhythmic patterns are part of an accretionary, down-state sequence developing from an alongshore beach state (longshore bar trough) following a storm event [Wright and Short, 1984]. Within the intermediate beach states, immediately after the longshore bar trough substate is the rhythmic bar and beach substate (crescentic bar), next the transverse bar and rip and finally the low tide terrace. Both the rhythmic bar and beach and transverse bar and rip substates are characterized by the presence of intense rip currents. Rip current systems often result in erosion features known as megacusps [Short and Hesp, 1982; Thornton

¹CNRS, UMR 5805 EPOC, Université de Bordeaux, Talence, France.

²Laboratoire des Ecoulements Géophysiques et Industriels (UJF-INPG-CNRS), Grenoble, France.

³UMR 5243, Université Montpellier 2, Montpellier, France.

et al., 2007]. Therefore, understanding and predicting rip current dynamics is relevant for shoreline evolution and localized beach and dune erosion [Thornton *et al.*, 2007]. In addition, rip currents are known to be a major hazard to beach users as they are the cause of the majority of rescues and fatalities within the beach environment [Short, 1999; Scott *et al.*, 2009]. Accordingly, rip currents also have significant implications from the perspective of beach safety and life guarding.

[4] A classic explanation for rip current generation is that rip current circulations are driven by alongshore variations of wave-induced radiation stress [Longuet-Higgins and Stewart, 1964]. These gradients can be due to spatial variability of the incident wavefield due to wave groups [Dalrymple, 1975], wave-current interactions [Dalrymple and Lozano, 1978], wavefield interaction with lower-frequency waves such as edge waves [Symonds and Ranasinghe, 2001] or local topographic variations [Bowen, 1969]. The latter is called “topographically controlled rip current,” while the three other ones refer to “transient rip currents” [Johnson and Pattiaratchi, 2004a]. More recently, using the general theoretical analysis of wave-driven currents and vortex dynamics due to dissipating waves by Buhler [2000], Bonneton *et al.* [2010] showed that wave-averaged vertical vorticity associated with rip current circulations are controlled by alongshore differential broken-wave energy dissipation. In this paper, we are essentially dealing with topographically controlled rip current systems, that is, rip current circulations that are guided and constrained by the 3-D surf zone sandbar morphology.

[5] Within the last decade, a significant number of field rip current investigations have been made [Aagaard *et al.*, 1997; Brander, 1999; Brander and Short, 2000, 2001; MacMahan *et al.*, 2004a, 2004b, 2005, 2008; Bruneau *et al.*, 2009b; MacMahan *et al.*, 2010; Austin *et al.*, 2010]. These wave-driven circulations were found to be strongly unstable and subject to pulsations over a large range of temporal scales. Rip current pulsations within the infragravity band have been widely observed. While groupiness of the incoming waves [Shepard and Inman, 1950] or infragravity standing waves [Sonu, 1972; MacMahan *et al.*, 2004a] were hypothesized to explain the presence of these pulsations, the causative mechanism has yet to be conclusively found. Pulsations at much lower frequency have also been reported [Smith and Largier, 1995; Brander and Short, 2001; MacMahan *et al.*, 2004b; Callaghan *et al.*, 2005; Bruneau *et al.*, 2009a; Reniers *et al.*, 2007]. Explanations based on shear instabilities, detached surf zone eddies in the rip head and rip circulation cell oscillations challenged over the past few years. Similarly, the causative mechanism of far-infragravity rip current pulsations has yet to be conclusively found. Of note, the spatial distribution of rip current circulation variability at these different temporal scales is poorly understood.

[6] Field rip current studies showed that rip currents are strongly influenced by tidal elevation with rip current activity and maximum rip current velocities around low tide in microtidal [Brander, 1999], mesotidal [Brander and Short, 2000] and macrotidal [Austin *et al.*, 2010] wave-dominated beaches. Conversely, on the meso-macrotidal high-energy Aquitanian Coast beaches (SW France), Bruneau *et al.*

[2009b] found that maximum rip current velocities shifted toward higher tides with increasing offshore wave height, corroborating earlier numerical exercises by Castelle and Bonneton [2006] and Castelle *et al.* [2006] on this stretch of coastline. Because of these persistent changes in tidal elevation and wave conditions, an in-depth investigation of rip current circulations as a function of beach morphology for a given wave condition and tidal elevation is a challenging task in the field. To overcome time varying both offshore wave conditions and tidal elevation, rip current intensity has mostly been investigated as a function of the dimensionless variable H/h (offshore wave height/water depth on the sandbar) which is considered as a measure of the forcing intensity. Not surprisingly, it was found that rip velocities increase with increasing wave height and decreasing water elevation. Conversely, the sensitivity of rip velocities to the relative depth of the rip channel for a given offshore wave condition and tidal elevation has barely been touched upon [Nielsen *et al.*, 2001] and is therefore poorly understood.

[7] A substantial number of laboratory experiments, all performed with a fixed bed, have been undertaken for easier grasping of topographically controlled rip current circulation information than on natural beaches. Eulerian measurements [Hamm, 1992; Haller and Dalrymple, 2001; Haas and Svendsen, 2002] and more recently Lagrangian techniques [Kennedy and Thomas, 2004] have been used to investigate rip current systems. The latter, when a sufficient number of drifters are released during a sufficient duration, can be transformed into a horizontal mean circulation field. The same drifter deployment strategy was recently attempted in the field by Schmidt *et al.* [2005], Austin *et al.* [2009], and MacMahan *et al.* [2010].

[8] A limitation of the existing laboratory experiments of rip current circulations is the configuration of beach used. While most of the field observations of rip currents were undertaken on incised rip channels inshore-connected shoals or depressions on near-planar beaches [MacMahan *et al.*, 2006] with low to pronounced alongshore nonuniformity, all laboratory measurements, with the exception of Hamm [1992], have been done with an alongshore bar-trough beach cut by a deep rip channel [Drønen *et al.*, 2002; Haas and Svendsen, 2002; Kennedy and Thomas, 2004; Kennedy *et al.*, 2006]. The resulting man-made beach shape in the laboratory resulted in rather unrealistic or very scarcely observed rip-channel morphologies. For instance, the relative depth of the rip channel is in general higher in laboratory (2.5–5) compared to the field (1.2–2.7; see the review of MacMahan *et al.* [2006]). Strong discontinuities in the seabed morphology were additionally observed during these previous laboratory experiments, which resulted in ubiquitous macrovortices being shed from the sharp bar crests in the vicinity of the rip channel and subsequently shed offshore [Kennedy *et al.*, 2006]. Generation of these macrovortices is likely to significantly alter the overall hydrodynamics [Chen *et al.*, 1999].

[9] In order to assess the sensitivity of mean rip current flow characteristics to beach morphology, this study describes a laboratory experiment of drifter observations over a moveable bed in the presence of rip current circulations. Flows across eight contrasting nature-like barred-

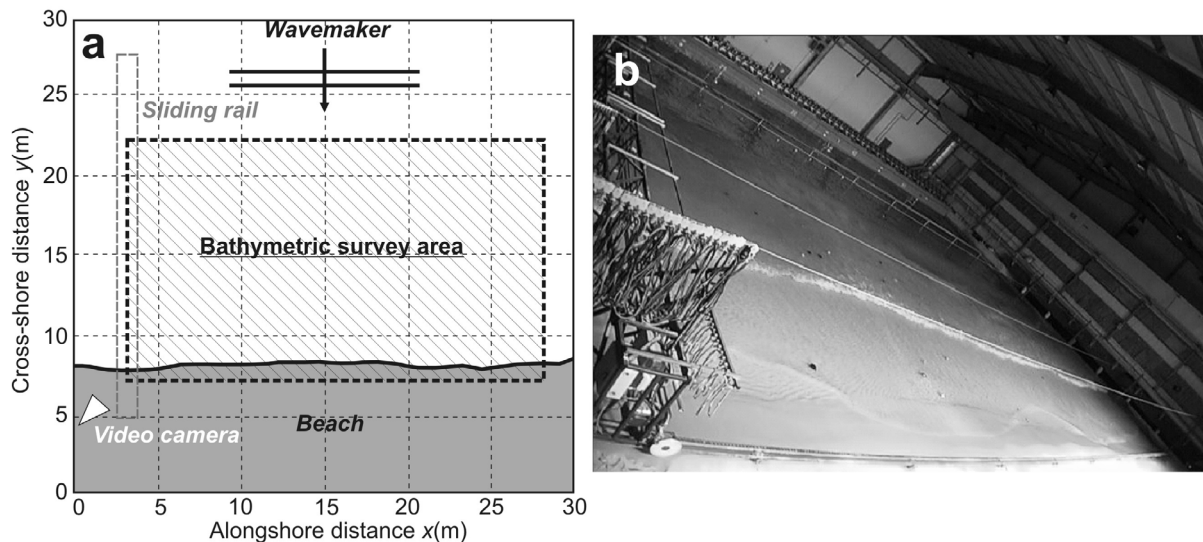


Figure 1. (a) Schematic of setup for the laboratory experiment with delimitations of the bathymetric survey area (dashed box) and location of the video camera. (b) Sample of captured video image with drifters.

beach morphologies consistent with the morphodynamic intermediate beach state classification of *Wright and Short* [1984] are investigated.

2. Experimental Setup

2.1. Laboratory Experiment

[10] The laboratory experiment [Michallet *et al.*, 2010] was undertaken during a 5 week period in a multidirectional wave basin at the SOGREAH (LHF facility, G-INP, France). The basin extended 30 m in both cross-shore (y axis) and alongshore (x axis) directions with an offshore wall constituted of 60 independently controlled piston-type wavemakers (Figure 1). The choice of the general experimental setup (wave conditions, offshore water depth, initial alongshore-uniform beach profile) was based on a previous laboratory experiment of intermediate cross-shore barred-beach morphodynamics in a 36 m long flume [Michallet *et al.*, 2007; Grasso *et al.*, 2009a, 2009b]. To move up to full scale, the length scaling factor and time scaling factor are 10 and 3, respectively. A complete description of the downscaling in hydrodynamics is presented by Grasso *et al.* [2009b]. The still water level at the wavemaker was $h_0 = 76.5$ cm and the mean beach slope was about $1/25$. The moveable bed consisted of fine sand with $d_{50} = 164 \mu\text{m}$ with sediment layer over the rigid bottom of at least 10 cm thick throughout the experiment.

[11] Shore-normal waves were used and the same wave conditions were applied for all cases presented in this paper. Irregular waves were generated according to a JONSWAP spectrum with a significant wave height $H_s = 18$ cm and a peak period $T_p = 3.5$ s. A linear combination of 350 random sinusoidal components was used to define a 20 min wave sequence. This wave sequence was repeated continuously during the experiment as much as desired. Over the experiment, waves were generated for 102 h [Michallet *et al.*, 2010]. There was neither wave absorption nor second-order correction on the wavemaker motions. Of note, because the

primary objective of the experiment was to investigate the formation and subsequent nonlinear evolution of 3-D surf zone sandbar, wave forcing at the wavemaker was not alongshore uniform to initiate sandbar instability. Two 0.5 m long independently controlled pistons centered at $x = 15$ m were set to half of the wave height at the other pistons. Preliminary investigations showed that, for an alongshore-uniform beach morphology, alongshore variations in wave height at the breaking point were small. Given the substantially alongshore nonuniform beaches investigated, wave-driven circulations were therefore assumed to be essentially guided and constrained by the 3-D sandbar morphology, with negligible effect of the alongshore nonuniform wave generation at the wavemaker.

[12] The seabed morphology was measured using a laser profiler mounted on a motorized trolley located on a sliding rail (Figure 1a). This measurement technique required emptying the basin before recording the bed elevation. During the experiment, the duration between each bathymetric survey varied from 7 to 26 twenty-minute wave sequences. The seabed elevation was recorded with millimeter accuracy every 10 cm and 1 cm in the alongshore and cross-shore direction, respectively. Ambient 3-D beach morphologies were not shaped by the investigators but formed through the positive feedback between flow (waves and currents) sediment transport and the evolving morphology from an initial alongshore-uniform beach geometry. As shown in Figure 1a the bathymetric survey zone was restricted by the sliding rail configuration and covered the area $3.12 \text{ m} < x < 28.02 \text{ m}$, $7.16 \text{ m} < y < 22.16 \text{ m}$. The beach morphology both seaward and shoreward of this area was reasonably alongshore uniform and did not evolve significantly throughout the experiment. The beach morphology appeared to be strongly variable during the experiment, ranging from an alongshore-uniform geometry to a well-developed bar-rip morphology, favoring a large range of rip current systems. The present study focuses on a specific period of the experiment when the formation and the subsequent disappearance of rip channels

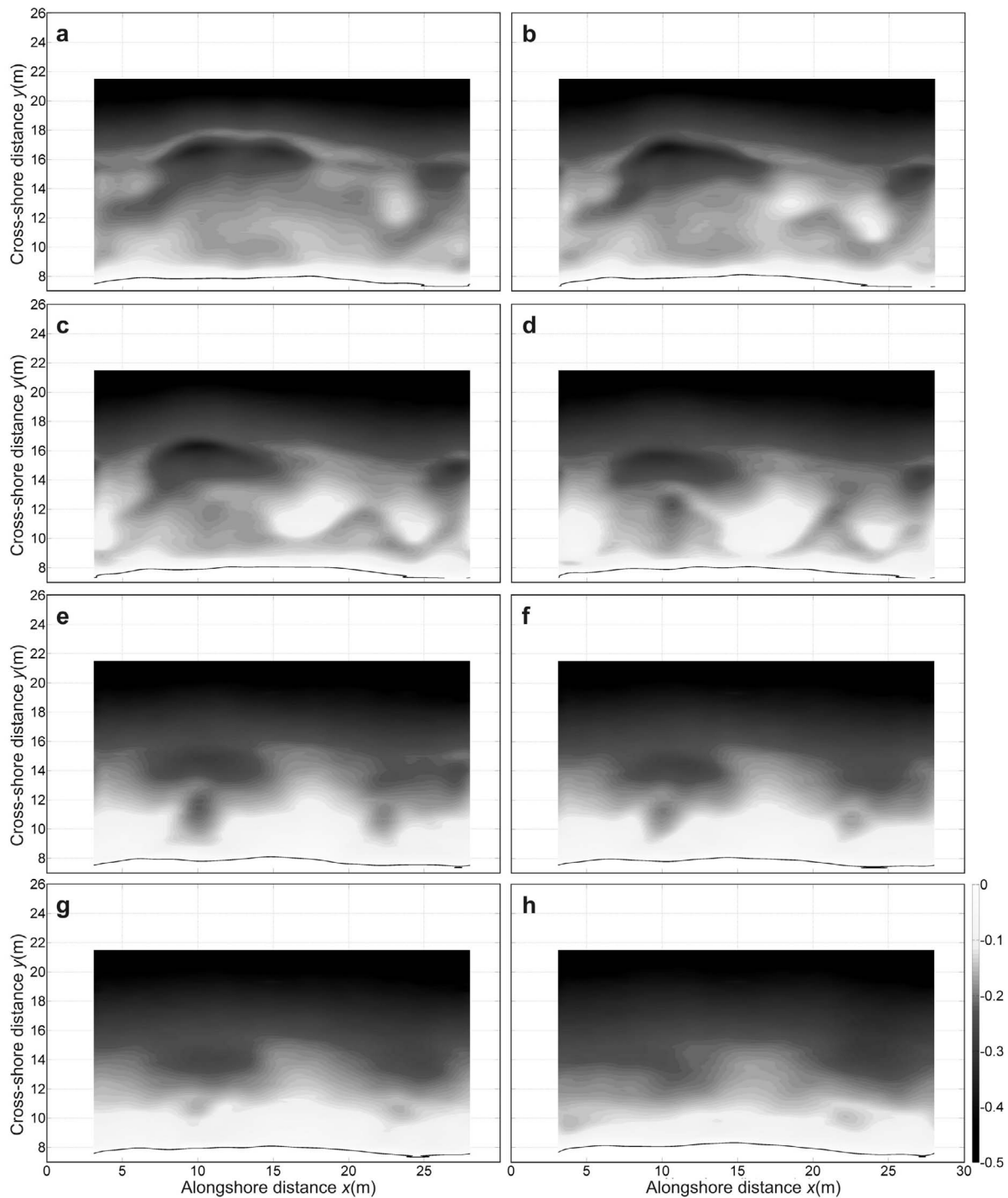


Figure 2. Beach morphologies surveyed with millimeter accuracy (ripples are filtered) corresponding to (a) Run A, (b) Run B, (c) Run C, (d) Run D, (e) Run E, (f) Run F, (g) Run G, and (h) Run H. Grayscale bar and solid black line indicate the seabed elevation in meters and the shoreline position, respectively.

were observed. This period coincided with the deployment of the largest number of drifters to be tracked by the video camera.

2.2. Beach Morphologies

[13] Eight beach morphologies (Figure 2) are considered to assess the rip current circulations as a function of the

seabed characteristics only, with corresponding alongshore-averaged beach profiles shown in Figure 3. Following the morphodynamic framework of *Wright and Short* [1984] for intermediate beach states, this morphological sequence appears as a down-state sequence. The beach initially exhibited a typical rhythmic bar and beach morphology (Figure 2a) with a single crescentic bar at about $4\text{ m} < x < 18\text{ m}$

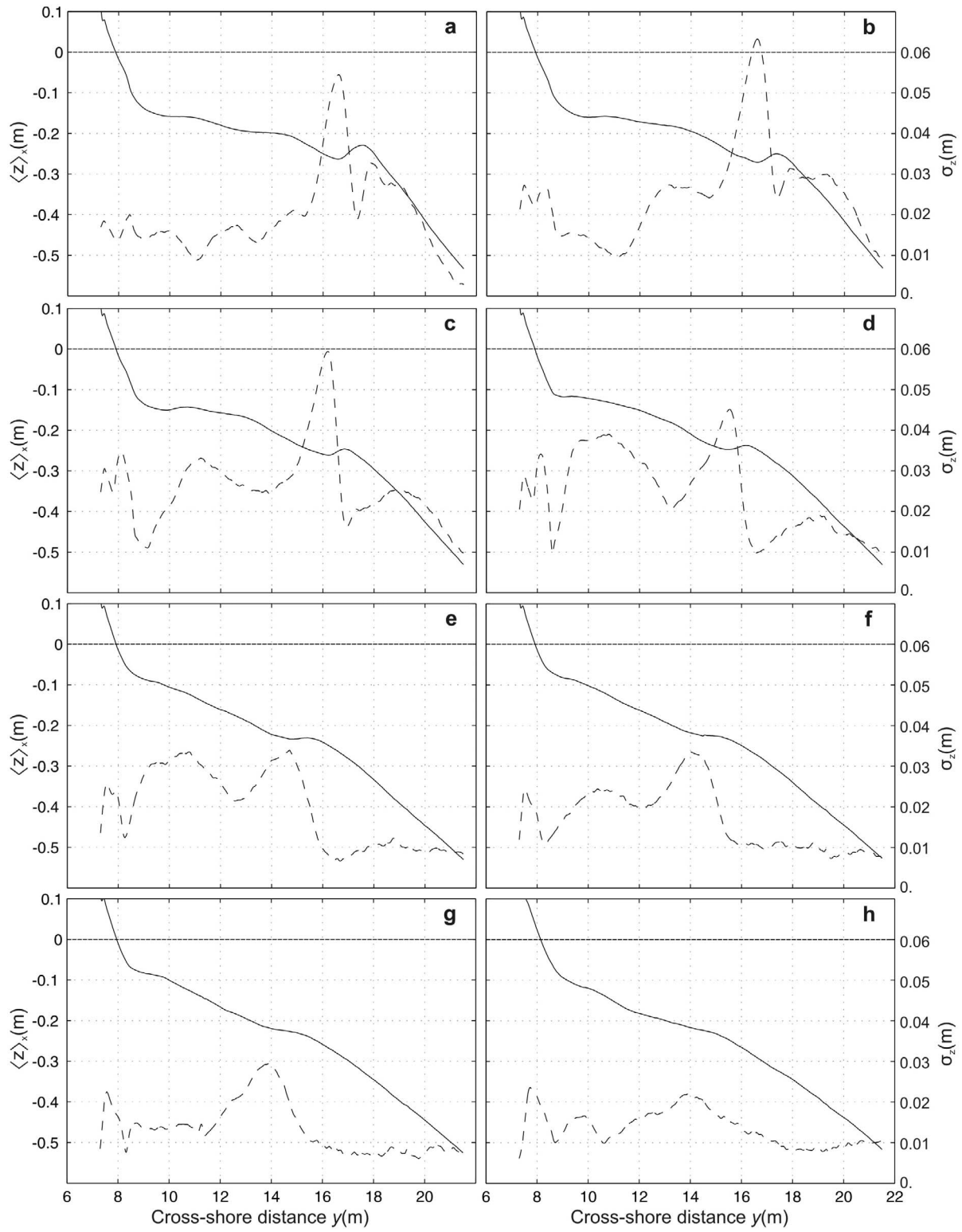


Figure 3. The mean cross-shore bottom profile $\langle z(y) \rangle_x$ (solid line) and its alongshore nonuniformities $\sigma_z(y)$ (dotted line) for (a) Run A, (b) Run B, (c) Run C, (d) Run D, (e) Run E, (f) Run F, (g) Run G, and (h) Run H.

that was not connected to the shore. The bar subsequently migrated shoreward (Figures 2b and 2c; see also Figures 3a–3c) and attached to the beach (Figure 2d) with the formation of shallow shoals alternating with 3 deeper rip channels (at about $x = 10$ m, 21 m and 26 m) associated with alongshore-oriented feeder channels typical of the transverse bar and rip morphology [Wright and Short, 1984]. The two rip channels at about $x = 22$ m and 26 m then merged to form a single rip channel at $x = 22$ m together with the infilling of the alongshore-oriented feeder channels (Figure 2e). The following beach morphology (Figure 2f), that can be similarly categorized into the transverse bar and rip morphology, show a continuous overall shoreward migration of the bar (Figure 3) together with the increasing discrimination between the two rip channels (Figure 2). The beach then progressively tended toward an almost featureless terrace-like morphology (Figures 2g and 2h) as the two previously observed rip channels were significantly infilled.

[14] During the whole sequence, the shoreline position did not change significantly. Of note, the beach morphologies in Figure 2 are similar to previously surveyed bar-rip morphologies in the field [see, e.g., Brander and Cowell, 2003] or recently surveyed crescentic sandbars [Almar et al., 2010]. Therefore, and conversely to earlier laboratory experiments, the morphologies were characterized by incised rip channels inshore-connected or unconnected shoals, without any sharp discontinuity in the seabed elevation. A preliminary analysis of all the bathymetry, that was corroborated by the observations during the experiment, showed the persistent presence of small-scale variations of the seabed elevation (on the order of 1–2 cm) which were related to the presence of ripples, suggesting bedload sediment transport ubiquity. In the following, ripples were filtered from the bathymetric data.

[15] In this paper we focus on the rip current system that was located at about $x = 10$ m as, throughout the experiment, both the highest rip current velocities and largest number of drifters were most of the time observed. To examine the evolution of the rip current characteristics as a function of the beach morphology, we quantified the beach geometry for the eight morphologies. While the relative depth of the rip channel has been previously widely used to characterize the rip channel three-dimensionality [MacMahan et al., 2006], here we used the more consistent measure of bathymetric nonuniformities, that is, the alongshore depth standard deviation $\sigma_z(y)$ [Feddersen and Guza, 2003; MacMahan et al., 2008]:

$$\sigma_z(y) = \sqrt{\frac{1}{x_2 - x_1} \int_{x_1}^{x_2} (z(x, y) - \langle z(y) \rangle_x)^2 dx} \quad (1)$$

where $z(x, y)$ is the seabed elevation at $7.16 \text{ m} < y < 22 \text{ m}$, $x_1 = 3.12 \text{ m}$ and $x_2 = 18 \text{ m}$, and $\langle z(y) \rangle_x$ is the alongshore mean cross-shore profile between x_1 and x_2 . This choice of x_1 and x_2 was motivated by the consideration of the rip current located at about $x = 11 \text{ m}$ that was hypothesized not to be significantly influenced by the beach morphology at $x > 18 \text{ m}$. Figure 3 shows the evolution of $\langle z(y) \rangle_x$ and $\sigma_z(y)$ during the experiment. Corroborating the previous qualitative description of the beach down-state transition in Figure 2, Figure 3 shows the persistent shoreward migration of the bar during the experiment. The beach alongshore nonuniformity is pre-

dominantly associated with crescentic patterns and rip morphology. For instance when a crescentic pattern is observed (Figure 2a), the maximum beach alongshore nonuniformity is characterized by two peaks located immediately seaward and shoreward of the bar crest at about $y = 17.5 \text{ m}$. This is consistent with the general observation of crescentic patterns that are usually viewed as an alongshore sequence of horns and bays alternating seaward and shoreward of the bar crest [Van Enckevort et al., 2004]. This two-peak feature is also readily apparent for the transverse bar and rip morphology (Figures 3c) with peaks located shoreward and seaward of the cross-shore location $y \approx 12\text{--}14 \text{ m}$. At the beginning of the sequence, $\sigma_z(y)$ significantly increases (Figures 3a and 3b) and subsequently decreases until the end of the sequence. In the following, we consider the cross-shore averaged beach alongshore nonuniformity $\overline{\sigma_z} = \langle \sigma_z(y) \rangle_y$ as the measure of the bar-rip system three-dimensionality.

2.3. Drifter Observations

[16] Motivated by previous drifter developments for both field and laboratory rip current studies [Schmidt et al., 2003; Johnson and Pattiaratchi, 2004a; Kennedy and Thomas, 2004; Schmidt et al., 2005], a few drifter designs and shapes were tested prior to the experiment. The best drifter design was a simple balloon filled of water (with a diameter between 5 and 10 cm). Various balloon colors were used for easier discrimination of drifter position when dense clusters were observed. Preliminary tests showed that broken and near-breaking waves passing over the drifters did not significantly push the drifters ashore (i.e., “surfing”). Drifters followed gross water motion in the top 5–10 cm of the water column, except for brief periods when the drifters would sink, when caught in a plunging breaker, and follow deeper portions of the water column for a few seconds. Only during very scarce events did a balloon blow up when caught by a plunging breaker. Note that wave breaking occurred within the rip channel during the higher portions of the wave group, even when the rip channel was the most developed. During the lower portion of the wave group wave breaking occurred in the rip channel only when the rip channel was significantly infilled (Runs G and H). The average surf zone width was about 10 m throughout the experiment.

[17] Drifters were deployed in the surf zone for each run for a 30 to 60 min duration. A bathymetric survey was undertaken immediately after each video run. Generally, wave trains were generated during a few hours between each video run so that the video run duration was short in comparison with timescales associated with the morphological evolution. Therefore the bathymetry was assumed not to change significantly during the video run and the observed rip currents are considered as representative of wave-driven circulations over the subsequently surveyed beach morphology.

[18] For most of the video runs, drifters were manually deployed ashore along the entire domain before the beginning of the wave sequence. Drifters were subsequently caught by the feeder currents and then spread within the surf zone by the wave-driven circulations. For the less-developed rip current systems, drifters were manually deployed at about 5 m seaward of the shoreline before the wave sequence and were further retrieved for redeployment when they came ashore and were trapped in the swash zone for more than about 5 min. Drifters that exited the surf zone and remained

Table 1. Video Run Conditions With the Beach Alongshore Nonuniformity $\overline{\sigma_z}$ and RBB, TBR, and LTT^a

	Run A	Run B	Run C	Run D	Run E	Run F	Run G	Run H
Video-run duration (min)	40	30	60	60	60	60	60	40
Number of deployed drifters	22	20	25	37	29	39	32	21
Beach morphology	RBB	RBB	TBR	TBR	TBR	TBR	LTT	LTT
$\overline{\sigma_z}$ (m)	0.0186	0.0258	0.0242	0.0224	0.0194	0.0167	0.0134	0.0135

^aRBB is rhythmic bar and beach, TBR is transverse bar and rip, and LTT is low tide terrace morphology [Wright and Short, 1984].

near $y > 22$ m were not retrieved for redeployment. Between 20 and 37 drifters were deployed for each video run. Table 1 lists video run conditions, with the eight video runs further denoted Run A to Run H in the paper.

[19] Drifters were tracked using captured images from a shore-mounted video camera with a captured image resolution of 720 by 576 pixels at 25 frames per second. Image coordinates were then rectified to still water level Cartesian coordinates (see Figure 1b for an example of captured image). Note that because of camera limitations and the presence of the sliding rail (Figure 1), it was impossible to track the drifters at alongshore distance of about $x < 5$ m. The image rectification to Cartesian coordinates was done using a three-dimensional direct linear transformation, the transformation coefficients being calculated by a least squares method on 29 ground control points. The lens optical distortion (radial) was also taken into account. The procedure mean error applied on the control points position is 0.11 m, with a maximum error of 0.26 m at the farther point of the domain. The pixel footprint ranged from less than 0.05 m at the bottom left-hand side of the beach to about 0.35 m at $(x, y) = (30 \text{ m}, 30 \text{ m})$. Within the investigated rip current system that was located close to the camera, the mean errors due to image rectification and identification of the center of the drifter are about 0.1 m and 0.15 m, respectively.

[20] Because of nonoptimized lightning in the laboratory, drifters were tracked using a semiautomatic method in order to avoid difficulties and errors induced by a full automatic method. For each drifter, the drifter position was indicated manually by mouse clicking every 6 s on the original video. Cross-shore and alongshore velocities were estimated from a linear interpolation in position and time of each sequential position of the drifter position at a 1 s time step over a 30 s duration. The study area was further divided into 1 m by 1 m bins in which, according to the drifter position information, the velocity data was sorted into the appropriate bin. Only bins with five or more independent velocity measurements were used for the data processing, which results in statistically confident results [Spydell *et al.*, 2006]. When a sufficient number of velocity measurements were available for a given bin and a required duration, mean current vectors and standard deviations in current angle and intensity were computed to grasp information on the spatial variability of the rip current circulation instabilities. As a drifter followed gross water motions it bobbed up and down with the incoming waves. It resulted in a rectified apparent horizontal motion of the drifter because of the oblique field of view. Some preliminary tests with mouse clicking every 0.2 s showed that these motions were smoothed by the interpolation. Given the quantified errors due to image rectification and identification of the drifter center, the typical maximum drifter velocity error is 0.05 m/s at the furthest basin corner, with a reasonable value of 0.025 m/s within the investigated rip current system.

For the mean velocity computations, the expected maximum error decreases with increasing number of samples and is estimated to be about 0.01 m/s when the minimum requirement of five individual measurements is met. Given that a large number of individual samples were systematically observed for a given bin in both the rip neck and within the rip cells (typically between 20 and 200 depending on the video run), the expected maximum error on mean velocity is assumed to be less than 10% of the typical mean velocity within the rip current system.

3. Results

3.1. General Drifter Behavior

[21] Wave-driven circulation patterns were strongly unstable throughout the experiment. Figure 4 shows a sequence of drifter tracks every 120 s for Run D over a well-developed bar-rip morphology with a pronounced shore-normal rip channel at about $x = 10$ m (Figure 2d). Overall, the trajectories show a well-defined offshore flow with two counterrotating cells (Figure 4), with most of the drifters being trapped within the circulations associated with the rip current centered in $x = 10$ m. These circular patterns are essentially coupled with the underlying morphology. Overall the two circulation cells equally occupied half of the shoal and rip channel. There was generally little longshore spreading of the drifters in the rip neck section, indicating a constrained jet-like flow. In contrast, in the rip head, drifters rapidly spread, showing significant variability over a very short distance. Most of the drifters slowly turned right or left with no apparent preference and were subsequently driven across the shoals at an average speed of about 0.1 m/s (instantaneous velocity up to about 0.15 m/s). Only a small number of drifters were ejected from the surf zone (Figures 4f, 4g, 4q, and 4r). When drifters exited the surf zone compartment, they were almost stationary and slowly exited the video camera field. Only a small number slowly turned shoreward before being subsequently caught once again within the rip current circulations, indicating very little onshore flow outside of the surf zone compartment. Rarely a drifter caught in the rip current located at $x = 10$ m was transported sufficiently rightward to be further caught in the rip current located at $x = 22$ m (see, for instance, Figure 4d), suggesting a rather small interchange of water between the two rip current systems. Note that it was not the case for all the video runs. Only three drifters remained ashore at the convergence of the two feeder currents at about $x = 10$ m during most of the sequence. All the other drifters that came ashore were usually rapidly caught by the feeder currents and further transported in the rip current.

[22] The rip jet sometimes changed direction from left to right. For instance, a significant leftward trend is observed at $t = 420\text{--}540$ s (Figure 4a) that rapidly changes to a rightward trend at $t = 660\text{--}780$ s (Figure 4c) and subsequently a leftward

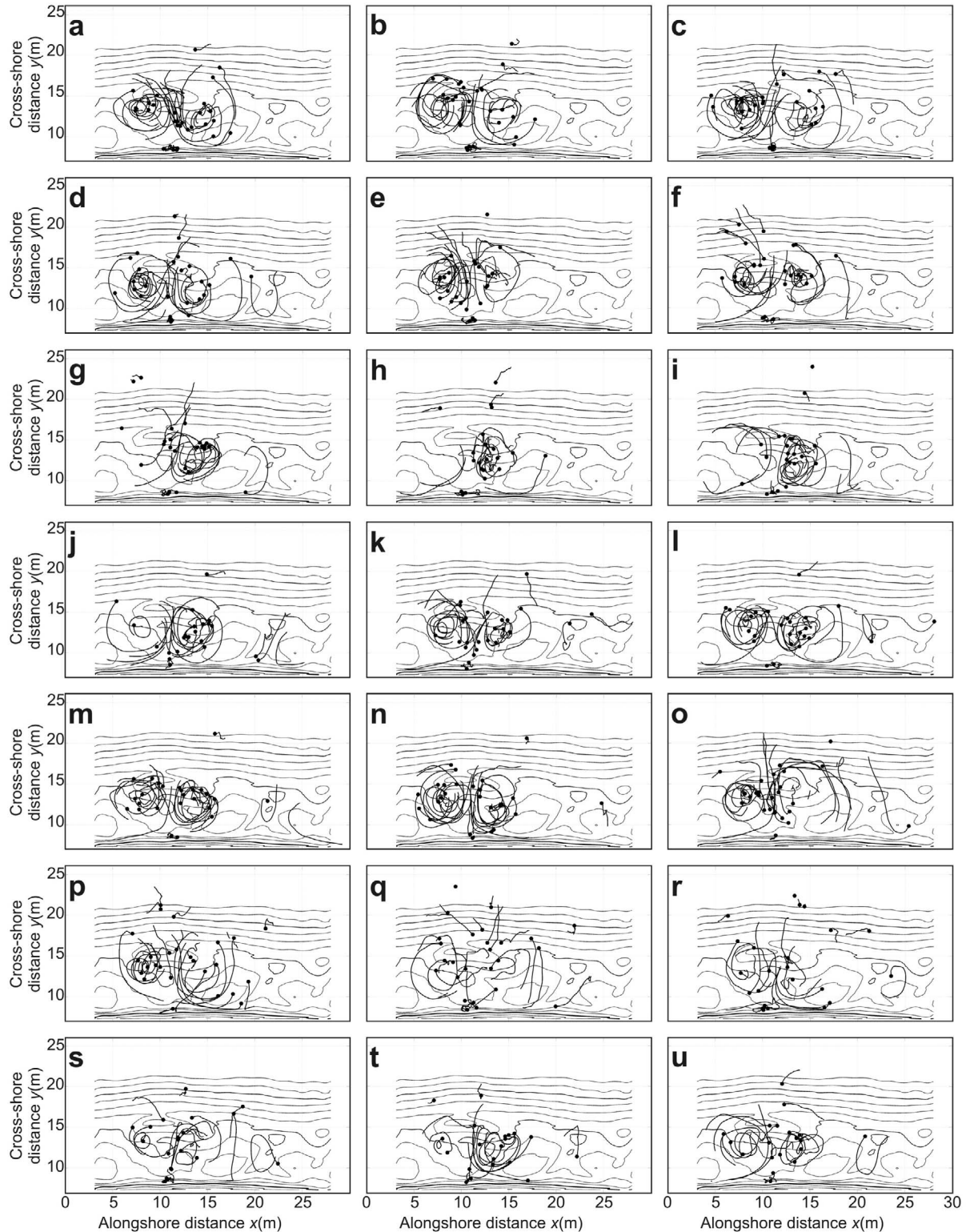


Figure 4. Startup pathlines of the drifters during Run D with the local bottom morphology contoured in the background. (a) 420–540 s, (b) 540–660 s, (c) 660–780 s, (d) 780–900 s, (e) 900–1020 s, (f) 1020–1140 s, (g) 1140–1260 s, (h) 1260–1380 s, (i) 1380–1500 s, (j) 1500–1620 s, (k) 1620–1740 s, (l) 1740–1860 s, (m) 1860–1980 s, (n) 1980–2100 s, (o) 2100–2220 s, (p) 2220–2340 s, (q) 2340–2460 s, (r) 2460–2580 s, (s) 2580–2700 s, (t) 2700–2820 s, and (u) 2820–2940 s. Solid circles give the starting point of each pathline. Drifters were manually deployed ashore at about $5 \text{ m} < x < 20 \text{ m}$ at $t = 0 \text{ s}$.

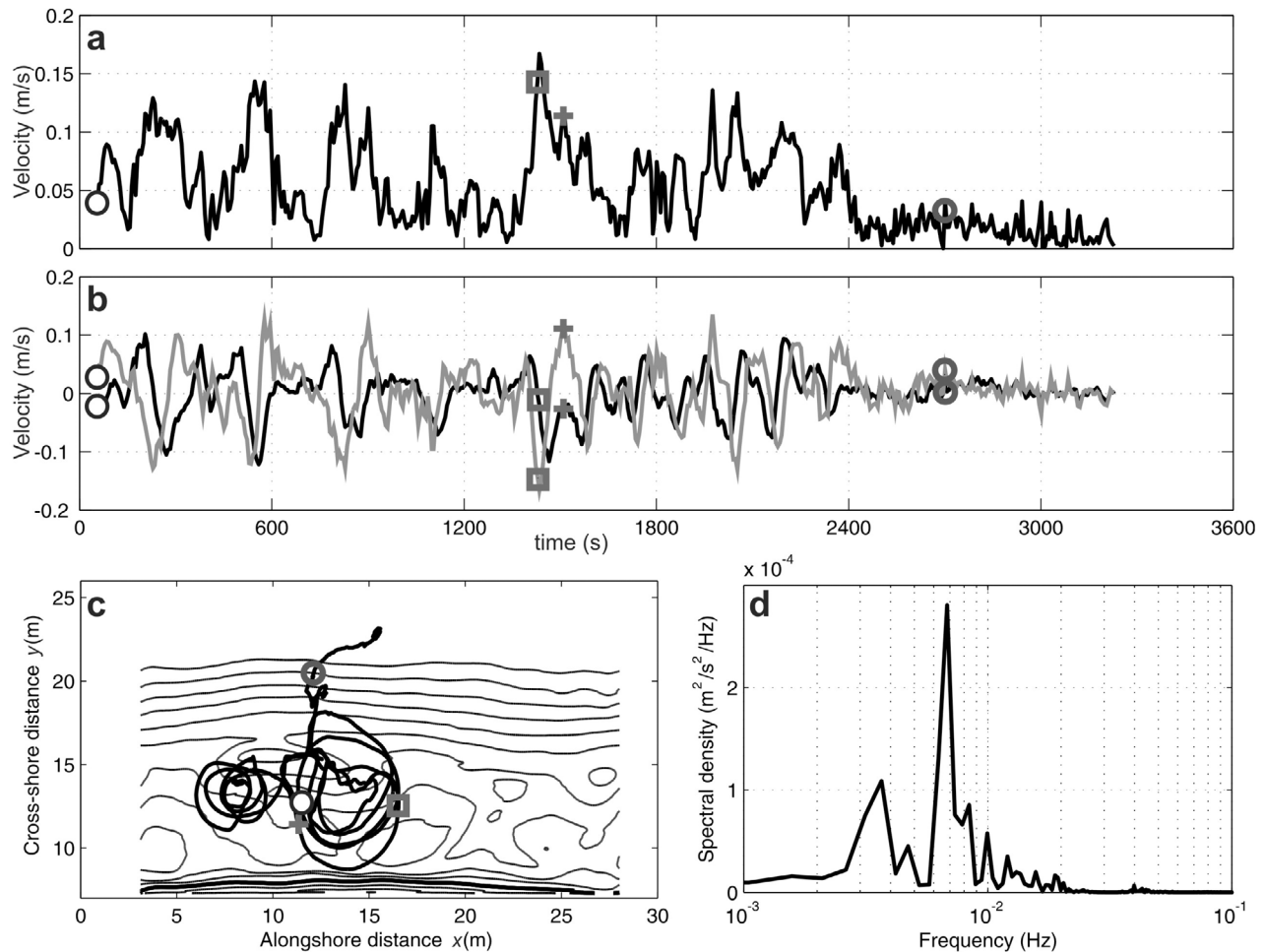


Figure 5. Single drifter data computed during Run D with (a) time series of the drifter velocity, (b) time series of the cross-shore velocity (gray line) and longshore velocity (black line), (c) drifter pathline with the local bottom morphology contoured in the background, and (d) corresponding energy spectrum for cross-shore velocity. In Figures 5a–5c the dark gray cross, circle, and square indicate velocities and locations of the drifter at three different times, and the black circle indicates the starting point.

trend at $t = 1020$ – 1140 s (Figure 4f). The circulation cells do not seem to migrate in the alongshore direction, whereas substantial cross-shore migration of the circulation cells is readily apparent. For instance, the rip current circulation centers seem to be located at about $y = 14$ m at $t = 1020$ – 1140 s (Figure 4f) or at $t = 2340$ – 2360 s (Figure 4q) while, most of the time, they appear to be located at about $y = 12$ – 13 m (Figure 4). Interestingly, this seaward migration of the rip current circulation seems to be associated with subsequent events of drifter expulsion from the surf zone compartment (see at $t = 1140$ – 1260 s in Figure 4g and $t = 2580$ – 2700 s in Figure 4s).

[23] Unlike other laboratory rip current studies, there was hardly obvious trace of smaller-scale vortices ($O(0.5$ – 1 m)) being shed offshore. This can be explained by the choice of our drifter track computation method. The combination of errors in the positioning, the tracking every 6 s and the interpolation in position in time to compute both velocities and tracks are expected to substantially filter these vortices.

[24] Drifters traveled in and out of any 1 m by 1 m bin at irregular intervals. Therefore, like previous field and labora-

tory rip current studies using Lagrangian measurements, it was impossible to obtain continuous time series of velocity at a given bin. On the other hand, it was possible to compute continuous time series of position and velocity of a given drifter. Figure 5 shows a selected drifter trajectory together with time series of cross-shore and longshore velocities. The selected drifter was initially deployed ashore and was subsequently retained within the rip current circulations. The drifter was caught about 10 times in the rip current and further transported in the rightward or leftward circulation with no apparent preference. As shown in the spectral density plot of the cross-shore velocity (Figure 5d) a clear peak appears at a frequency of about $f = 0.007$ Hz which means that the selected drifter undertook a full rip current circulation every 2–3 min. The selected drifter was subsequently ejected from the surf zone at about $t = 2400$ s (Figure 5c). Maximum velocities of about 0.15 m/s were reached when the drifter was in the rip neck or over the shoal (Figures 5a and 5b). Interestingly, the selected drifter did not experience a high offshore-directed velocity in the rip neck immediately before exiting the surf zone (less than

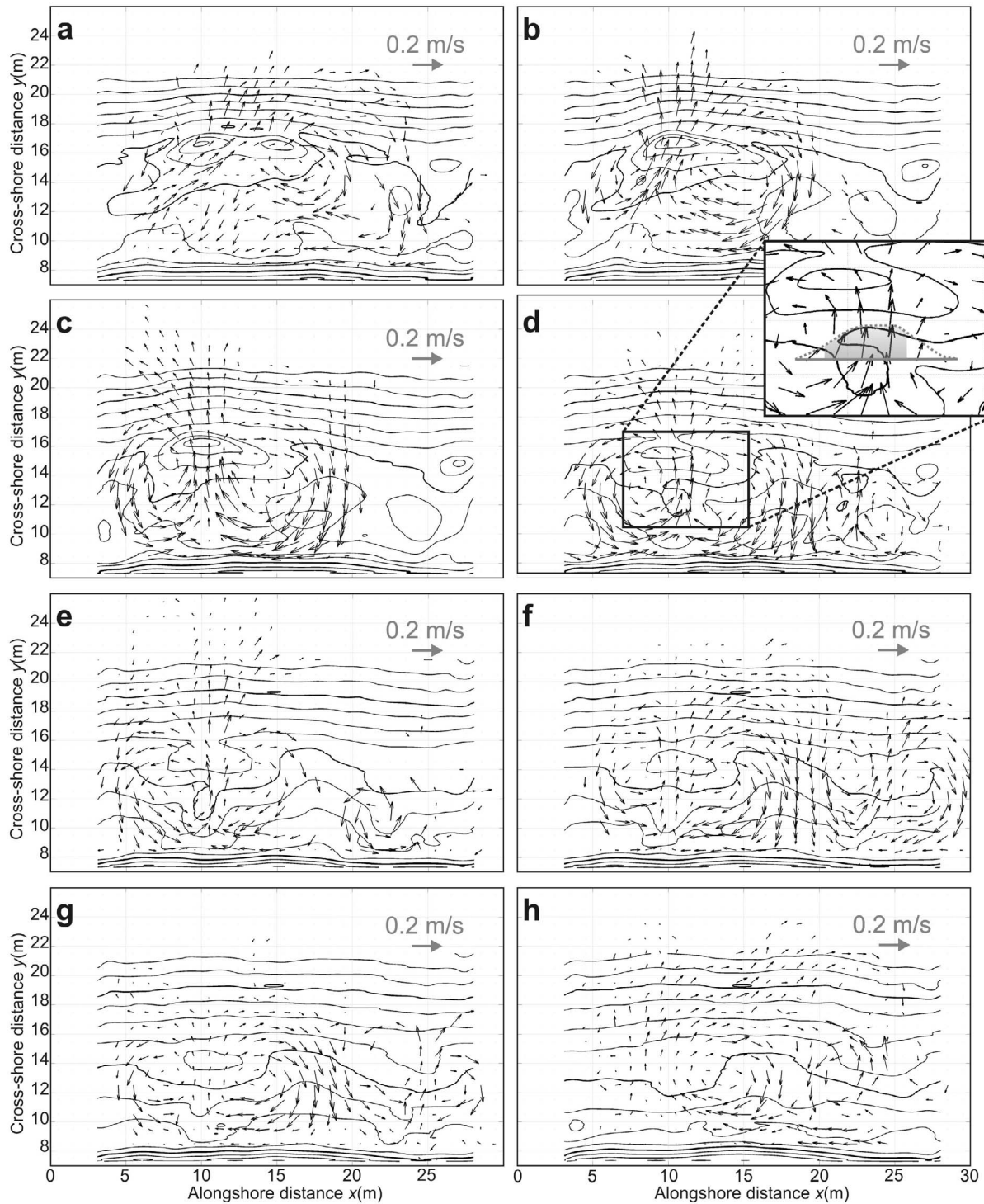


Figure 6. Computed mean flow patterns plotted over the bathymetry for the eight situations (a) Run A, (b) Run B, (c) Run C, (d) Run D, (e) Run E, (f) Run F, (g) Run G, and (h) Run H. Grid spacing resolution is 1 m in both x (cross-shore) and y (alongshore) directions. The local bottom morphology is contoured in the background. The methodology used to compute rip current velocity U_{rip} is shown in Figure 6d and is further detailed in the text.

0.1 m/s, see Figure 5a at $t \approx 2400$ s), which goes against the common perception [Smith and Largier, 1995; Reniers et al., 2007] that drifters exiting the surf zone are systematically caught by a pulsating jet.

3.2. Mean Rip Current Circulations

[25] As indicated in section 3.2, rip current circulations were unstable and the velocities were exposed to long-period

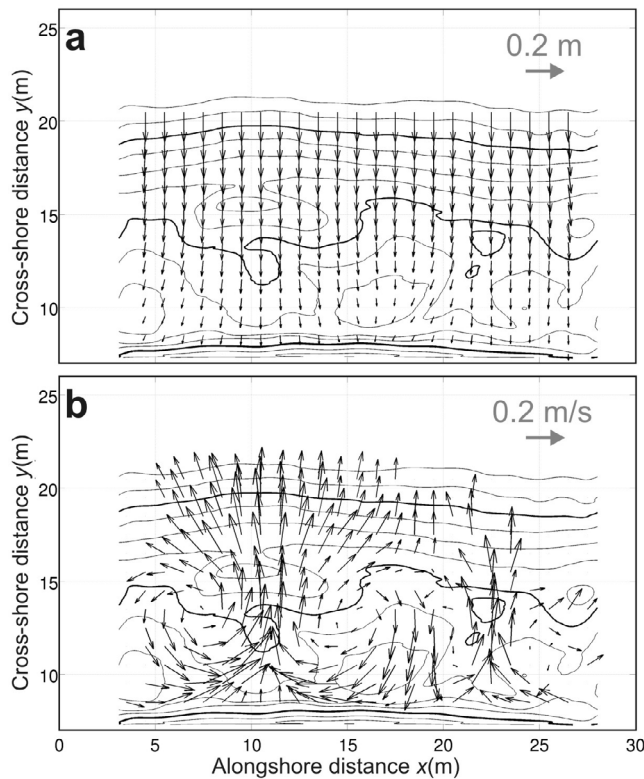


Figure 7. (a) Root-mean-square wave height vector field ($H_{rms}\vec{e}_k$) simulated for Run D with (b) resulting Eulerian velocity field. The local bottom morphology is contoured in the background.

oscillations. The video run durations were long enough to capture a large number of low-frequency periods and, therefore, mean values computed below are assumed not to be affected by infragravity and far-infragravity motions. Figure 6 shows the computed mean rip current circulations for the eight beach morphologies given in Figure 2. Classic rip current patterns are observed for each with alongshore feeder currents, a reasonably intense and narrow offshore-directed jet in the channel, strong onshore-directed flow across the shoals and counterrotating cells to the left and right of the rip current. Only one rip current is observed in the A and B video runs (Figures 6a and 6b) that were constrained by the single crescentic pattern. For all the other video runs two rip current systems are visible at $x \approx 10$ m and $x \approx 23$ m. Note that additional cells closer to the shoreline were persistently seen in previous laboratory experiments over alongshore bar-trough profiles cut by a rip channel [Drønen *et al.*, 2002; Haas and Svendsen, 2002; Kennedy and Thomas, 2004] and further confirmed through numerical modeling over similar beach geometries [Haas *et al.*, 2003; Kennedy *et al.*, 2006]. Such circulation cells rotating in the opposite direction of the bar/rip channel circulation were only observed for Run A with a single cell centered at about ($x = 8$ m, $y = 12$ m) when the crescentic bar was sufficiently detached from the beach (Figure 6a).

[26] Because of the contrasting beach morphologies, mean rip current circulation patterns strongly evolved during the course of the experiment. Consistent with the general field observation, rip current intensity readily increases with

increasing beach three-dimensionality. More importantly, rip current shape varied from shore-normal (Figures 6d–6h) to strongly skewed rightward (Figures 6a and 6b) and weakly skewed leftward (Figure 6c). The rip current skewness during the first part of the experiment is essentially due to along-shore variability of water depth above the shoals.

[27] From run A to run D, onshore- and offshore-directed flows in the rip channel and on the shoals were in the same order of magnitude (0.1–0.2 m/s). In contrast, when the rip current started to significantly decrease in intensity (Run E, Figure 6e) onshore flows only slightly decreased in intensity (0.1–0.15 m/s) while offshore-directed flows substantially decreased up to being negligible during in Run H (Figure 6h). Similarly to onshore-directed flows, feeder currents only slightly weakened throughout the morphological down-state sequence meanwhile feeder channels appear to have disappeared by Run E. Outside of the breaking region, that is at about $y > 18$ –20 m, the computed mean offshore-directed flows are expected to be overestimated because data at these locations was available almost only during events of drifter ejection from the surf, which is not likely to be representative of the overall hydrodynamics at these locations.

[28] Because of persistent changes in waves and tidal conditions in the field and the unrealistic beach geometries in laboratory experiment, rip current intensity U_{rip} has only been quantified as a function of the relative depth of the rip channel or the dimensionless variable H/h representative of the forcing intensity. Because rip current circulations are controlled by alongshore differential broken-wave energy dissipation [Bonneton *et al.*, 2010] that results from non-uniformities of the bathymetry, here we quantify the rip current intensity as a function of the beach alongshore nonuniformity, defined as $\bar{\sigma}_z$ the cross-shore averaged beach alongshore nonuniformity $\sigma_z(y)$ given in equation (1).

[29] In Figure 6, flow patterns were presented using the mean measured drifter velocities. As detailed in [Kennedy and Thomas, 2004], measured drifter velocities can significantly differ from true Eulerian velocities because of Stokes drift as drifters responded to orbital motions. We estimated Stokes drift using the spectral wave model SWAN [Booij *et al.*, 1999] to compute the root mean square wave height H_{rms} within the domain for the eight beach morphologies. Default values were chosen in the model with no account for wave-current interactions because of a lack of mean flow information over the whole domain. We estimated the Lagrangian Stokes drift on the drifters using the small-amplitude theory,

$$\vec{U}_{LD} = \frac{ga^2k \cosh 2kh}{C} \vec{e}_k \quad (2)$$

where g is the gravitational acceleration, a the wave amplitude deduced from H_{rms} , k the wave number, h the local water depth, C is the phase speed and \vec{e}_k the unit vector along wave rays. We subsequently removed the Stokes drift component to the mean drifter velocities to compute the estimated Eulerian velocity field. Figure 7 shows the computed wavefield and resulting mean Eulerian velocity field for Run D (Figure 6d). Note that seaward of the surf zone, at locations where finite amplitude effects (e.g., depth-induced breaking) are not consistent with small amplitude wave theory, the Stokes drift is likely to be significantly overestimated

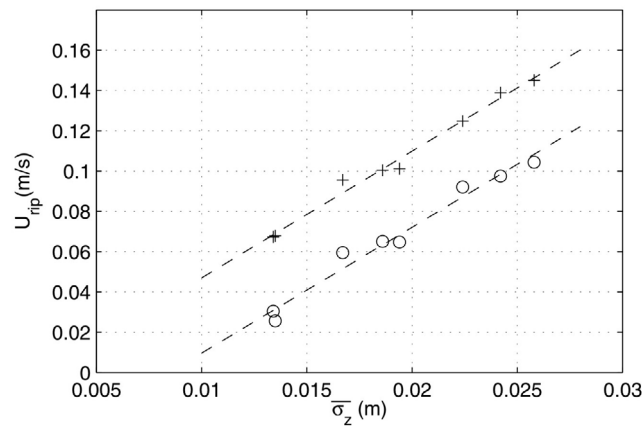


Figure 8. Rip current velocity U_{rip} without (circles) and accounting for (crosses) Stokes drift versus beach alongshore nonuniformity σ_z . The dashed lines represent linear interpolation.

[Kennedy and Thomas, 2004]. Within the rip current circulation, the computed velocities are assumed to be representative of the mean Eulerian velocities.

[30] Defining rip current velocity U_{rip} is not that straightforward, especially because strong changes in the general flow structure can occur with the evolving bathymetry, which was the case during our laboratory experiment (Figure 6). Some considerations had to be made on what definition of U_{rip} should be used, that is, where in the rip flow structure to pick up the measurements. Only in the work by Drønen *et al.* [2002] the idealized beach shape together with persistent shore-normal rip current made it natural to define U_{rip} current as the value of the rip current velocity at its maximum. Surprisingly, there was no further discussion on a more generic definition of U_{rip} in the literature than “flow intensity in the rip channel.”

[31] Obviously both definitions are hardly applicable herein. For instance during Run B (Figure 6b) the rip current is strongly skewed rightward with both maximum flow velocity and offshore-directed component maximum at ($x = 6.5$ m, $y = 10.5$ m) which is not located in the rip channel. Maximum offshore velocity is also found to be located significantly shoreward of the cross-shore position of the rip current circulation centers (located at about $x = 15$ m, Figure 6b), that is, almost in the feeder current. In contrast maximum offshore velocity is located significantly seaward of the cross-shore position of the rip current circulation centers during Run H (Figure 6h). Therefore, we had to find a consistent definition of U_{rip} based on the geometry of the rip current circulation structure.

[32] We defined U_{rip} as the mean offshore-directed flow along the 3 m long section where the offshore-oriented flow velocity is maximum across the alongshore section joining the two circulation cell centers (see Figure 6d). The two circulation cell centers were manually detected. The choice of a 3 m length was motivated by having a sufficient number of bins to have a representative measure of the offshore flow and avoiding potential odd data at a given bin. Accordingly our computed U_{rip} is substantially less intense than maximum rip current intensity in the rip throat. Figure 8 shows both U_{rip} , with and without accounting for Stokes drift, as a function of

beach alongshore nonuniformity $\bar{\sigma}_z$. The overall trend corroborates both the observations in Figure 6 and previous works in the field and in the laboratory as U_{rip} increases with increasing beach alongshore nonuniformity. More importantly, U_{rip} linearly increases with increasing $\bar{\sigma}_z$. Relationship is statistically very good as the R^2 coefficient of determination is 0.97 and 0.98 not accounting and accounting for Stokes drift, respectively. Results are synthesized in Table 2.

[33] The Froude number (Fr), is used to quantify the dimensionless rip current intensity:

$$Fr = \frac{U_{rip}}{\sqrt{gh}} \quad (3)$$

where h is the mean local water depth across the same 3 m section as that along which U_{rip} has been computed. According to MacMahan *et al.* [2006] rip current can be classified into the low-energy ($Fr < 0.1$), moderate-energy ($0.1 < Fr < 0.35$) and high-energy ($Fr > 0.35$) regimes. In the present study, Fr at a given bin in the rip neck region (larger than the 3 m averaged given in Table 2) showed $0.5 < Fr < 1.2$ throughout the experiment, which means that rip currents were within the low- to moderate-energy regime. This suggests weak wave-current interactions throughout our experiment and therefore supports the disregard of wave-current interaction in our SWAN computations.

3.3. Spatial Variability of Rip Current Circulation Infragravity and Far-Infragravity Motions

[34] Information on the spatial variability on how the flow patterns are unstable can be grasped through the standard deviation (σ) of the flow intensity and angle. Because standard deviation is very sensitive to the number of observations at a given bin, there is a strongly varying accuracy in the estimate of the variance. Accordingly, below standard deviations are mostly described in terms of patterns. The patterns of standard deviation of flow intensity (Figures 9a–9h) show that when rip current circulations were the most intense (Figures 9b–9d), highest variations in flow intensity are almost found systematically in the rip neck, suggesting the presence of strong rip current pulsations (on the order of 0.05 m/s). Slightly lower flow intensity variations are found within the rip current circulations throughout the experiment. There is hardly contrasting patterns in flow intensity standard deviation between the eight situations as maximum standard deviations are systematically found in the rip neck and at the onshore flow across the bar. This contrasts with the patterns of standard deviation of velocity angle (Figures 9i–9p). For instance Figure 9 reveals that rip current angle standard deviation within the rip neck increases with

Table 2. Beach Alongshore Nonuniformity $\bar{\sigma}_z$ and Mean Rip Current Characteristics for the Eight Situations With U_{rip} , U_{rip}^e , and Fr^{ea}

	Run A	Run B	Run C	Run D	Run E	Run F	Run G	Run H
$\bar{\sigma}_z$ (m)	0.0186	0.0258	0.0242	0.0224	0.0194	0.0167	0.0134	0.0135
U_{rip} (m/s)	0.0650	0.1044	0.0975	0.0921	0.0647	0.0595	0.0304	0.0256
U_{rip}^e (m/s)	0.1004	0.1450	0.1389	0.1248	0.1012	0.0956	0.0673	0.0679
Fr^{ea}	0.0631	0.0945	0.0997	0.0884	0.0724	0.0691	0.0475	0.0459

^a U_{rip} is the Lagrangian rip current intensity, U_{rip}^e is the Eulerian rip current intensity, and Fr^{ea} is the nondimensional measure of the Eulerian rip current intensity.

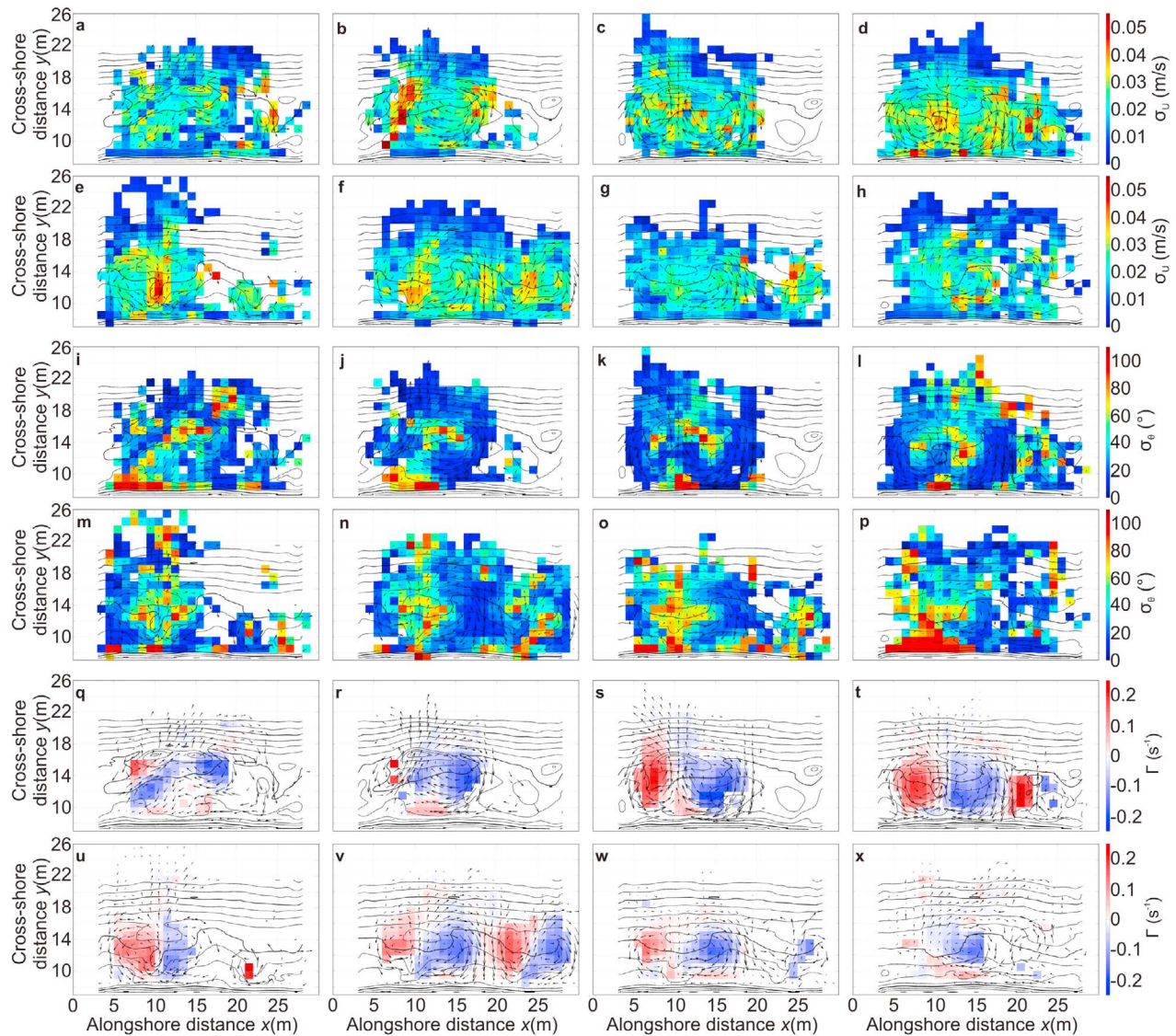


Figure 9. (a–h) Standard deviation of drifter velocity intensity σ_U for (a) Run A, (b) Run B, (c) Run C, (d) Run D, (e) Run E, (f) Run F, (g) Run G, and (h) Run H. (i–p) Standard deviation of drifter velocity angle σ_θ for (i) Run A, (j) Run B, (k) Run C, (l) Run D, (m) Run E, (n) Run F, (o) Run G, and (p) Run H. (q–x) Mean vorticity Γ estimated from drifter observations for (q) Run A, (r) Run B, (s) Run C, (t) Run D, (u) Run E, (v) Run F, (w) Run G, and (x) Run H.

decreasing rip current intensity. When the rip current was the most intense (Figures 9j–9l) the standard deviation of the flow angle within the rip neck is nonsignificant, typical of a highly pulsating and weakly directionally variable offshore-directed flow. Within the rip neck, the flow angle standard deviation increases with decreasing rip current intensity (Figures 9m–9p), which is typical of a reasonably pulsating and highly directionally variable offshore-directed flow. These observations suggest that rip current instabilities display contrasting behavior as a function of how the rip current is intense and sheared. However, the spatial variability in flow angle standard deviation for the eight situations shows some similarities. Flow direction appears rather constant in the feeders and over the shoals where strong alongshore and onshore currents are observed, respectively. This contrasts with the highly variable flow direction within the circulation cells. High standard

deviations of flow angle are also observed in the rip head area, because of the observed change of flow direction from left to right that was described in section 3.1. Overall, considering the two counterrotating circulation cells, lower standard deviation of flow angle occurs along the outer edges of the rotational elements (except for weak rip currents for which high standard deviations can be found in the rip neck), with the highest standard deviation occurring both near the circulation centers and in the vicinity of the rip head.

[35] A classic way to investigate rip current circulation characteristics is examining the vertical vorticity defined by $\Gamma = \nabla \wedge \bar{u}$, where \bar{u} is the mean flow velocity vector. Here Γ was computed in discrete form using a weighted central difference detailed by MacMahan *et al.* [2010]. The resulting vorticity patterns for the eight situations (Figures 9q–9x) show that the vorticity fields are rather typical in pattern with,

generally, maximum absolute vorticity occurring near the center of the circulation cells. In the rip current neck the vorticity was systematically very low. In contrast, the vorticity drastically increases immediately leftward or rightward of the rip neck. While it was not readily apparent when observing mean flow patterns in Figure 6, Figure 9 actually shows in some cases the presence of four quadrant circulation similar to the observation over bar-trough beach cut by a rip channel [Kennedy and Thomas, 2004]. Closer to the shoreline opposite-sign (weak) vorticity were sometimes observed (for instance, in Figures 9q, 9r, 9w, and 9x). Of note, areas with high absolute vorticity are observed in the same locations of the highest standard deviation of flow angle (Figure 9).

4. Discussion and Conclusions

[36] In contrast to earlier laboratory rip current studies, beach morphologies were essentially similar to previous observations of both bar-rip morphologies and crescentic patterns in the field. As far as we are concerned, drifter data gathered during runs A and B are the first flow measurement over crescentic bar systems to date. The seabed varied from reasonably alongshore uniform to strongly alongshore non-uniform with typical rhythmic bar and beach, transverse bar and rip and terrace-like features, representative of the range of sandbar shapes observed within the intermediate beaches [Wright and Short, 1984].

[37] As detailed in previous field and laboratory rip current studies based on Lagrangian measurements, drifter design is very important from the perspective of the representativeness of the true near-surface Lagrangian velocity. The most important issue in drifter design is usually addressing the problem of surfing in breaking waves [Schmidt et al., 2003; Johnson and Pattiaratchi, 2004b; MacMahan et al., 2009]. Because here we did not have to implement a global positioning system inside the drifter, we chose simple balloons filled of water to minimize surfing as drifters followed gross water motion in the top 5–10 cm of the water column with the same density as that of the water. Throughout the experiment, the visual observation of the drifters in breaking waves was that the balloons were extremely effective in resisting surfing. The only situation in which the drifters did not perform well was when caught at the plunge point of a strongly plunging wave and was subsequently exposed to sinking during 1–2 s. In the rip neck, drifters could rapidly migrate seaward even during the higher portion of the wave group. When approaching the same region, drifters could sometimes stop altogether, but this was visually independent of the presence of breaking or nonbreaking waves. Accordingly, the use of balloons as convenient and low-cost Lagrangian drifters in this laboratory study was successful.

[38] As shown in Figure 5 for the well-developed bar-rip morphology, drifters generally looped back into the same location of the circulation cell after about 140 s (0.007 Hz, Figure 4d). Moving up to full scale means that it would take about 7–8 min to loop back in the field for similar conditions (beach morphology and wave forcing). This is corroborated by recent drifter experiments on an open coast beach at Monterey in similar settings [MacMahan et al., 2010].

[39] Contrary to previous views, and corroborating recent both field experiment of drifter deployment in rip current systems [MacMahan et al., 2010] and numerical modeling

[Reniers et al., 2009], only a small number of drifters entering in the rip actually exited the surf zone. As shown in Figure 5, the selected drifter entered 10 times in the rip before exiting the surf zone compartment, which is in agreement with the study of MacMahan et al. [2010], who found that only about 10%–20% of the drifters caught in the rip exited the surf zone. The selected drifter did not experience a high offshore-directed velocity in the rip neck immediately before exiting the surf zone (less than 0.1 m/s, see Figure 5a at $t \approx 2400$ s) in comparison with the general 0.1–0.15 m/s velocity in the rip neck. This is intriguing as it was previously hypothesized in the literature [Smith and Largier, 1995; Reniers et al., 2007] that drifters exiting the surf zone compartment are systematically caught by a pulsating jet. Some drifters (not presented herein) were actually caught by a pulsating jet before exiting the surf zone but this was by far nonsystematic. Interestingly, the selected drifter that exited the surf zone in Figure 5c has been likely caught in a vortex being shed offshore as it can be deduced from the looped track at about ($x = 12.5$ m, $y = 18$ m). This applied for many drifter expulsions throughout the experiment supporting the idea that ejection of surf zone material occurs when surf zone eddies temporarily extend the rip current beyond the surf zone and subsequently detach [Reniers et al., 2010]. Our laboratory rip current study therefore supports recent field and numerical study [MacMahan et al., 2010; Reniers et al., 2010] suggesting that rip flow does not exit the surf zone as much as previously thought and instead is maintained within the surf zone through circulation cells and vorticity. This goes against the traditional paradigm of rip current flow that is now challenged by field, numerical and laboratory studies. Extensive assessment of surf zone retention during this experiment will be explored elsewhere.

[40] According to the morphological framework of Wright and Short [1984], here we observed three typical intermediate beach substates that are almost systematically observed along wave-dominated beaches, that are, the rhythmic bar and beach (RBB), transverse bar (TBR) and rip and terrace-like (LTT) morphologies. While the classification of Wright and Short [1984] provided very comprehensive qualitative description of the hydrodynamics over these 3-D nearshore patterns, here for the first time quantitative data is provided considering shore-normal constant wave forcing. The present data highlights some contrasting behavior of rip current kinematics depending on the beach morphology. Only low-energy rip currents are driven by waves over LTT morphologies. For the same shore-normal wave conditions rip current circulations are more intense over TBR and RBB morphologies with the presence of classic rip current patterns with counterrotating cells and a relatively narrow offshore-directed varying from shore-normal to potentially strongly skewed. Overall, our measurements are consistent with the qualitative description by Wright and Short [1984] except that we suspect that rip current circulations over crescentic patterns are potentially more intense than rip currents over transverse bar and rip morphologies if depth-induced wave breaking is sufficiently intense across the bar. This may also apply to bar and rip morphologies comprising shore-nonconnected shoals. Overall, we found that rip current intensity increases with the beach morphology moving from an alongshore-uniform geometry to a RBB state. For a given

wave height, maximum rip current intensity is observed when the bar is about to attach to the beach. Rip current intensity further decreases with the beach morphology moving from a TBR to a LTT state.

[41] Of note, our results are also in agreement with the model of *Wright and Short* [1984] for the low tide terrace configuration. We measured substantially smaller rip current intensity in Runs G and H, which goes with the usual weak, shallow and ephemeral description of “minirips” in low tide terrace settings [*Wright and Short*, 1984]. This however goes against the observations of *Brander* [1999] who measured increasing rip current intensity from a transverse bar and rip morphology to a low tide terrace morphology on a very similar field situation. The reason for this contrasting behavior remains unclear. Two potential explanations, among others, can be proposed here. First, offshore wave angle to the shore is crucial to the rip current system, which was not assessed by *Brander* [1999] because wave data was non-directional. Second, the current meter was close to the shore and rather far from the rip throat for the LTT morphology by *Brander* [1999]. The measured cross-shore velocity may have captured undertow and/or feeder effects. Because the pioneer work of *Brander* [1999] contains the only existing field measurements of an evolving rip current during a down-state sequence, our study motivates future intensive field observations of evolving rip currents encompassing a down-state sequence. This will require intensive drifter deployments to accurately capture the entire rip current circulations and subsequently accurately quantify rip current intensity.

[42] In this study we proposed a slightly different definition of rip current intensity than in previous studies. This definition is essentially based on the rip current geometry which can be easily applied elsewhere if there are a sufficient number of available flow measurements. Only using this definition, rip current intensity was found to linearly increase with increasing beach alongshore nonuniformity. This striking relationship was only found within the low- to moderate-energy rip current regime, therefore it has to be extended and confronted with other field and laboratory rip current studies to also further take into account wave period and wave angle to the shore. Given the recent advances in nearshore bathymetry estimation through assimilation of model computations and remote observations [*Van Dongeren et al.*, 2008], beach alongshore nonuniformity could eventually lead to a good predictor of rip current velocity in the field which is of interest from the perspective of beach safety.

[43] The mean vertical vorticity field Γ has been computed for the eight situations (Figures 9q–9x). Despite vorticity fields do not cover the entire domain, from these computations it is readily apparent that Γ increases with beach alongshore nonuniformity. This relationship can be enlightened by the analysis of the mean flow vertical vorticity equation given by *Bonneton et al.* [2010],

$$\frac{\partial \Gamma}{\partial t} + \vec{\nabla} \cdot (\Gamma \vec{U}) = \vec{\nabla} \wedge (D \vec{e}_k) + \tau_t \quad (4)$$

where \vec{U} is the mean transport horizontal velocity, D is the intensity of the depth-induced breaking dissipative force and τ_t the turbulent diffusion of the vorticity. For quasi-stationary rip current circulations ($\partial \Gamma / \partial t \approx 0$), the nonlinear advective term $\vec{\nabla} \cdot (\Gamma \vec{U})$ becomes small in comparison with the wave-

induced vorticity forcing term $\vec{\nabla} \wedge (D \vec{e}_k)$ [*Bonneton et al.*, 2010] that can be further approximated as $\vec{\nabla} D \wedge \vec{e}_k \sim -\partial D / \partial y$ if neglecting wave refraction. This results in a balance between wave-induced vorticity $-\partial D / \partial y$, the alongshore differential broken-wave energy dissipation essentially caused by alongshore depth variations, and the turbulent diffusion of the vorticity $\tau_t \sim \nu_t \vec{\nabla}^2 \Gamma$ where ν_t is a turbulent eddy viscosity. As wave dissipation is larger across the shoals than across the rip channel, $-\partial D / \partial y$ drives the strength and the sign of the wave-driven circulation rotational nature (Figure 9).

[44] Despite that it does not provide any information on the involved temporal scales (infragravity or far infragravity), computed standard deviations of flow intensity and direction provide high-resolution information on the spatial variability of the rip current circulation variations. For instance for intense rip current over a RBB or TBR morphology, we highlighted highly pulsating and weakly directionally variable offshore-directed flow in the rip channel, which contrasts with weakly pulsating and highly directional variable flows within the circulation cells. Overall lower standard deviation of flow angle occurs along the outer edges of the rotational elements (except for weak rip currents for which high standard deviations can be found in the rip neck), with the highest standard deviation occurring near the circulation centers and in the vicinity of the rip head. Our laboratory study suggests that spatial distribution of infragravity and far-infragravity motions in rip current settings can vary significantly depending on the rip current regime.

[45] To date the present experiment is the first one involving flow measurements together with an evolving nature-like 3-D sandy beach morphology for a given wave condition and water elevation. Some of the results presented herein are essentially similar to recent field rip current studies, for instance when dealing with surf zone retention and rip current circulations, which brings high confidence in our laboratory results. The data gathered herein will also be eventually used to build a benchmark for the validation of wave-driven circulation and Boussinesq-type models as well as nonlinear morphodynamic models. Our study therefore tends to promote the combination of field, numerical and physical studies to better understand rip current circulations as well as how they interact with the evolving beach morphology.

[46] **Acknowledgments.** This work was undertaken within the framework of the Project MODLIT (RELIEFS/INSU, SHOM-DGA) with additional financial support from COPTER (ANR). BC acknowledges support from BARBEC (ANR). The authors greatly acknowledge SOGREAH Consultants for sharing their facility and for technical support when constructing the physical model, especially the assistance provided by G. Excoffier and L. Marcellin. The authors are also thankful to all the people involved in this experiment. The research presented in this paper was also stimulated by recent fruitful discussions during the First International Rip Current Symposium held in Miami in February 2010. We appreciate the valuable comments by the two anonymous reviewers for making this a better manuscript.

References

- Aagaard, T., B. Greenwood, and J. Nielsen (1997), Mean currents and sediment transport in a rip channel, *Mar. Geol.*, *140*, 24–45.
- Almar, R., B. Castelle, B. G. Ruessink, N. S en echal, P. Bonneton, and V. Marieu (2010), Two- and three-dimensional double-sandbar system behaviour under intense wave forcing and a meso-macro tidal range, *Cont. Shelf Res.*, *30*, 781–792.

- Austin, M., T. M. Scott, J. W. Brown, J. A. Brown, and J. H. MacMahan (2009), Macro-tidal rip current experiment: Circulation and dynamics, *J. Coastal Res.*, *SI 56*, 24–28.
- Austin, M., T. M. Scott, J. W. Brown, J. A. Brown, J. H. MacMahan, G. Masselink, and P. Russell (2010), Temporal observations of rip current circulation on a macro-tidal beach, *Cont. Shelf Res.*, *30*, 1149–1165.
- Bonneton, P., N. Bruneau, B. Castelle, and F. Marche (2010), Large-scale vorticity generation due to dissipating waves in the surf zone, *Discrete Contin. Dyn. Syst., Ser. B*, *13*(4), 729–738.
- Booij, N., R. C. Ris, and L. H. Holthuisen (1999), A third-generation wave model for coastal regions: 1. Model description and validation, *J. Geophys. Res.*, *104*, 7649–7666.
- Bowen, A. J. (1969), Rip currents: 1. Theoretical investigations, *J. Geophys. Res.*, *74*, 5467–5478.
- Brander, R. W. (1999), Field observations on the morphodynamic evolution of a low-energy rip current system, *Mar. Geol.*, *157*, 199–217.
- Brander, R. W., and P. J. Cowell (2003), A trend-surface technique for discrimination of surf-zone morphology: Rip current channels, *Earth Surf. Processes Landforms*, *28*, 905–918.
- Brander, R. W., and A. D. Short (2000), Morphodynamics of a large-scale rip current system at Muriwai Beach, New Zealand, *Mar. Geol.*, *165*, 27–39.
- Brander, R. W., and A. D. Short (2001), Flow kinematics of low-energy rip current systems, *J. Coastal Res.*, *17*, 468–481.
- Bruneau, N., B. Castelle, P. Bonneton, and R. Pedreros (2009a), Very low frequency motions of a rip current system: observation and modeling, *J. Coastal Res.*, *SI 56*, 1731–1735.
- Bruneau, N., B. Castelle, P. Bonneton, R. Pedreros, R. Almar, N. Bonneton, P. Bretel, J. P. Parisot, and N. Sénéchal (2009b), Field observations of an evolving rip current on a meso-macro-tidal well-developed inner bar and rip morphology, *Cont. Shelf Res.*, *29*, 1650–1662.
- Buhler, O. (2000), On the vorticity transport due to dissipating or breaking waves in shallow water flows, *J. Fluid Mech.*, *407*, 235–263.
- Callaghan, D. P., T. E. Baldock, P. Nielsen, D. M. Hanes, K. A. Haas, and J. H. MacMahan (2005), Pulsing and circulation in a rip current system, in *Coastal Engineering 2004: Proceedings of the 29th International Conference*, vol. 2, edited by J. M. Smith, pp. 1493–1505, World Sci., New York.
- Castelle, B., and P. Bonneton (2006), Modelling of a rip current induced by waves over a ridge and runnel system on the Aquitanian Coast, France, *C. R. Geosci.*, *338*, 711–717.
- Castelle, B., P. Bonneton, N. Sénéchal, H. Dupuis, R. Butel, and D. Michel (2006), Dynamics of wave-induced currents over an alongshore non-uniform multiple-barred sandy beach on the Aquitanian Coast, France, *Cont. Shelf Res.*, *26*, 113–131.
- Castelle, B., P. Bonneton, H. Dupuis, and N. Sénéchal (2007), Double bar beach dynamics on the high-energy meso-macro-tidal French Aquitanian Coast: A review, *Mar. Geol.*, *245*, 141–159.
- Chen, Q., R. A. Dalrymple, J. T. Kirby, A. B. Kennedy, and M. C. Haller (1999), Boussinesq modelling of a rip current system, *J. Geophys. Res.*, *104*, 20,617–20,637.
- Dalrymple, R. A. (1975), A mechanism for rip current generation on an open coast, *J. Geophys. Res.*, *80*, 3485–3487.
- Dalrymple, R. A., and C. Lozano (1978), Wave current interaction model for rip current, *J. Geophys. Res.*, *83*, 6063–6071.
- Drønen, N., H. Karunarathna, J. Fredsøe, B. M. Sumer, and R. Deigaard (2002), An experimental study of rip channel flow, *Coastal Eng.*, *45*, 223–238.
- Falqués, A., G. Coco, and D. A. Huntley (2000), A mechanism for the generation of wave-driven rhythmic patterns in the surf zone, *J. Geophys. Res.*, *105*, 24,071–24,088.
- Fedderson, F., and R. T. Guza (2003), Observations of nearshore circulation: Alongshore uniformity, *J. Geophys. Res.*, *108*(C1), 3006, doi:10.1029/2001JC001293.
- Grasso, F., H. Michallet, R. Certain, and E. Barthélemy (2009a), Experimental flume simulation of sandbar dynamics, *J. Coastal Res.*, *SI 56*, 54–58.
- Grasso, R., H. Michallet, E. Barthélemy, and R. Certain (2009b), Physical modeling of intermediate cross-shore beach morphology: Transient and equilibrium states, *J. Geophys. Res.*, *114*, C09001, doi:10.1029/2009JC005308.
- Haas, K. A., and I. A. Svendsen (2002), Laboratory measurements of the vertical structure of rip currents, *J. Geophys. Res.*, *107*(C5), 3047, doi:10.1029/2001JC000911.
- Haas, K. A., I. A. Svendsen, M. Haller, and Q. Zhao (2003), Quasi 3D modeling of rip current systems, *J. Geophys. Res.*, *108*(C7), 3217, doi:10.1029/2002JC001355.
- Haller, M., and R. A. Dalrymple (2001), Rip current instabilities, *J. Fluid Mech.*, *433*, 161–192.
- Hamm, L. (1992), Directional nearshore wave propagation over a rip channel: An experiment, in *Coastal Engineering, 1992: Proceedings of the 23rd International Conference, October 4–9, 1992, Venice, Italy*, edited by B. L. Edge, pp. 226–239, Am. Soc. of Civ. Eng., New York.
- Holman, R. A., G. Symonds, E. B. Thornton, and R. Ranasinghe (2006), Rip spacing and persistence on an embayed beach, *J. Geophys. Res.*, *111*, C01006, doi:10.1029/2005JC002965.
- Johnson, D., and C. Pattiaratchi (2004a), Transient rip currents and nearshore circulation on a swell-dominated beach, *J. Geophys. Res.*, *109*, C02026, doi:10.1029/2003JC001798.
- Johnson, D., and C. Pattiaratchi (2004b), Application, modelling and validation of surfzone drifters, *Coastal Eng.*, *51*, 455–471.
- Kennedy, A. B., and D. Thomas (2004), Drifter measurements in a laboratory rip current, *J. Geophys. Res.*, *109*, C08005, doi:10.1029/2003JC001927.
- Kennedy, A. B., M. Brocchini, L. Soldini, and E. Gutierrez (2006), Topographically controlled, breaking-wave-induced macrovortices. Part 2. Changing geometries, *J. Fluid Mech.*, *559*, 57–80.
- Longuet-Higgins, M. S., and R. W. Stewart (1964), Radiation stress in water waves; A physical discussion, with applications, *Deep Sea Res. Oceanogr. Abstr.*, *11*(4), 529–563.
- MacMahan, J. H., A. J. H. M. Reniers, E. B. Thornton, and T. P. Stanton (2004a), Infragravity rip current pulsations, *J. Geophys. Res.*, *109*, C01033, doi:10.1029/2003JC002068.
- MacMahan, J. H., A. J. H. M. Reniers, E. B. Thornton, and T. P. Stanton (2004b), Surf zone eddies coupled with rip current morphology, *J. Geophys. Res.*, *109*, C07004, doi:10.1029/2003JC002083.
- MacMahan, J. H., E. B. Thornton, T. P. Stanton, and A. J. H. M. Reniers (2005), RIPEX-observations of a rip current system, *Mar. Geol.*, *218*, 113–134.
- MacMahan, J. H., E. B. Thornton, and A. J. H. M. Reniers (2006), Rip current review, *Coastal Eng.*, *53*, 191–208.
- MacMahan, J. H., E. B. Thornton, A. J. H. M. Reniers, T. P. Stanton, and G. Symonds (2008), Low-energy rip currents associated with small bathymetric variations, *Mar. Geol.*, *255*, 156–164.
- MacMahan, J. H., J. W. Brown, and E. B. Thornton (2009), Low-cost handheld global positioning system for measuring surf-zone currents, *J. Coastal Res.*, *25*, 744–754.
- MacMahan, J. H., et al. (2010), Mean lagrangian flow behavior on an open coast rip channeled beach: A new perspective, *Mar. Geol.*, *268*, 1–15.
- McKenzie, P. (1958), Rip-current systems, *J. Geol.*, *66*, 103–113.
- Michallet, H., F. Grasso, and E. Barthélemy (2007), Long waves and beach profile evolutions, *J. Coastal Res.*, *SI 50*, 221–225.
- Michallet, H., B. Castelle, F. Bouchette, A. Lambert, C. Berni, E. Barthélemy, P. Bonneton, and D. Sous (2010), Modélisation de la morphodynamique d'une plage barrée tridimensionnelle (in French), *Proc. Journée Natl. Génie Côtier-Génie Civ.*, *11*, 379–386, doi:10.5150/jngcgc.2010.045-M.
- Nielsen, P., R. W. Brander, and M. G. Hughes (2001), Rip currents: Observations of hydraulic gradients, friction factors and pump efficiency, in *Coastal Dynamics '01: Proceedings of the Fourth Conference on Coastal Dynamics, June 11–15, 2001, Lund, Sweden*, edited by H. Hanson and M. Larson, pp. 483–492, Am. Soc. Civ. Eng., New York.
- Reniers, A. J. H. M., J. H. MacMahan, E. B. Thornton, and T. P. Stanton (2007), Modeling of very low frequency motions during RIPEX, *J. Geophys. Res.*, *112*, C07013, doi:10.1029/2005JC003122.
- Reniers, A. J. H. M., J. H. MacMahan, E. B. Thornton, T. P. Stanton, M. Henriquez, J. W. Brown, J. A. Brown, and E. Gallagher (2009), Surf zone retention on a rip-channelled beach, *J. Geophys. Res.*, *114*, C10010, doi:10.1029/2008JC005153.
- Reniers, A. J. H. M., J. H. MacMahan, F. J. Beron-Vera, and M. J. Olascoaga (2010), Rip-current pulses tied to Lagrangian coherent structures, *Geophys. Res. Lett.*, *37*, L05605, doi:10.1029/2009GL041443.
- Schmidt, W. E., B. T. Woodward, K. S. Millikan, R. T. Guza, and B. Raubenheimer (2003), A GPS-tracked surf zone drifter, *J. Atmos. Oceanic Technol.*, *20*, 1069–1075.
- Schmidt, W. E., R. T. Guza, and D. N. Slinn (2005), Surf zone currents over irregular bathymetry: Drifter observations and numerical simulations, *J. Geophys. Res.*, *110*, C12015, doi:10.1029/2004JC002421.
- Scott, T. M., P. Russell, G. Masselink, and A. Woolers (2009), Rip current variability and hazard along macro-tidal coast, *J. Coastal Res.*, *SI 56*, 895–898.
- Shepard, F. P., and D. L. Inman (1950), Nearshore water circulation related to bottom topography and wave refraction, *Trans. Am. Geophys. Union*, *31*, 196–212.
- Shepard, F. P., K. O. Emery, and E. C. La Fond (1941), Rip currents: A process of geological importance, *J. Geol.*, *49*, 337–369.
- Short, A. D. (1999), Beach hazards and safety, in *Handbook of Beach and Shoreface Morphodynamics*, edited by A. D. Short, pp. 292–304, John Wiley, Chichester, U. K.
- Short, A. D., and P. A. Hesp (1982), Wave, beach and dune interactions in South Eastern Australia, *Mar. Geol.*, *48*, 259–284.

- Smith, J. A., and J. L. Largier (1995), Observation of nearshore circulation: Rip currents, *J. Geophys. Res.*, *100*, 10,967–10,975.
- Sonu, C. J. (1972), Field observation of nearshore circulation and meandering currents, *J. Geophys. Res.*, *77*, 3232–3247.
- Spydell, M., F. Feddersen, and R. T. Guza (2006), Observing surf-zone dispersion with drifters, *J. Phys. Oceanogr.*, *37*, 2920–2939.
- Symonds, G., and R. Ranasinghe (2001), On the formation of rip currents on a plane beach, in *Coastal Engineering 2000: Conference Proceedings, July 16–21, 2000, Sydney, Australia*, edited by B. L. Edge, pp. 468–481, Am. Soc. of Civ. Eng., Reston, Va.
- Thornton, E. B., J. H. MacMahan, and A. H. Sallenger Jr. (2007), Rip currents, mega-cusps, and eroding dunes, *Mar. Geol.*, *240*, 151–167.
- Van Dongeren, A. R., N. G. Plant, A. B. Cohen, J. A. Roelvink, M. C. Haller, and P. Catalán (2008), Beach Wizard: Nearshore bathymetry estimation through assimilation of model computations and remote observations, *Coastal Eng.*, *55*, 1016–1027.
- Van Enckevort, I. M. J., B. G. Ruessink, G. Coco, K. Susuki, I. L. Turner, N. G. Plant, and R. A. Holman (2004), Observations of nearshore crescentic sandbars, *J. Geophys. Res.*, *109*, C06028, doi:10.1029/2003JC002214.
- Wright, L. D., and A. D. Short (1984), Morphodynamic variability of surf zones and beaches: A synthesis, *Mar. Geol.*, *56*, 93–118.
-
- E. Barthélemy, C. Berni, A. Lambert, and H. Michallet, Laboratoire des Ecoulements Géophysiques et Industriels (UJF-INPG-CNRS), BP53, F-38041 Grenoble Cedex, France.
- P. Bonneton, B. Castelle, B. Dubardier, F. Leckler, and V. Marieu, CNRS, UMR 5805 EPOC, Université de Bordeaux, Avenue des Facultés, F-33405 Talence Cedex, France. (b.castelle@epoc.u-bordeaux1.fr)
- F. Bouchette, UMR 5243, Université Montpellier 2, Place E. Bataillon, F-34095 Montpellier Cedex 5, France.